Electroconvection in nematic mixtures of bent-core and calamitic molecules

Shingo Tanaka and Hideo Takezoe
Department of Organic and Polymeric Materials, Tokyo Institute of Technology, 2-12-1 S8-Ookayama, Meguro-Ku, Tokyo 152-8552, Japan

Nándor Éber, Katalin Fodor-Csorba, Anikó Vajda, and Ágnes Buka
Research Institute for Solid State Physics and Optics, Hungarian Academy of Sciences, P.O. Box 49, H-1525 Budapest, Hungary
(Received 16 April 2009; published 10 August 2009)

The onset of electroconvection in binary mixtures of a bent-core and a rodlike nematic has been characterized by measuring the threshold voltage U_c and the critical wave number of the pattern in a wide range of frequencies f. In the mixtures rich in bent-core molecules, a "conductive-prewavy2-patternless-prewavy1" morphological sequence has been detected with an unusual negative slope of $U_c(f)$ at high frequencies. This latter scenario seems to be related to the bent-core component, as it disappears with increasing the concentration of rodlike molecules. In addition, one of the parameters most relevant for electroconvection, the electrical conductivity, has also been varied by ionic salt doping. It has been found that the above effect of the banana-shaped molecules on the electroconvection scenarios can be suppressed by the conductivity.

DOI: 10.1103/PhysRevE.80.021702 PACS number(s): 61.30.Gd, 47.54.−r, 47.20.Lz

I. INTRODUCTION

Liquid crystals made of achiral bent-core molecules have drawn considerable attention in the last decade due to their ability to form unconventional "banana" phases, including those with polar packing and ferroelectric switching and those exhibiting spontaneous chiral domain segregation [1]. The bent molecular structure may, moreover, lead to extraordinary properties even in the conventional mesophases; e.g., bent-core nematics are regarded as candidates for exhibiting a long-searched biaxial nematic phase [2,3]. A giant flexoelectricity [4] as well as some unprecedented behaviors of electroconvection patterns [5] have also been reported recently in a bent-core nematic.

Electroconvection (EC) is a pattern-forming instability of a homogeneous nematic liquid crystal layer which involves electric field induced director deformation with an associated charge separation and flow [6]. The resulting patterns have a great morphological richness. At onset, they mostly appear in the form of regular convection rolls. Their wave number $|\mathbf{q}|$ might cover a wide range depending on the material parameters and on the frequency f and the rms value U of the applied voltage [7]. As for the direction of the critical wave vector $\mathbf{q_c}$ at onset one has to distinguish between normal rolls (NRs) which are perpendicular to the initial director $\mathbf{n}$ ($\mathbf{q_c} \| \mathbf{n}$), oblique rolls (ORs) which run in two degenerate directions thus forming zigzag structures, and longitudinal rolls (LRs) with $\mathbf{q_c}$ (nearly) perpendicular to $\mathbf{n}$.

EC patterns can also be classified [7] according to whether their mechanism of formation can be (standard EC) or cannot be (nonstandard EC) interpreted by the standard model (SM) of electroconvection (i.e., by the combination of equations of nematodynamics with electrodynamics assuming Ohmic conduction) [8]. The most common examples of standard EC (the "conductive" OR and NR, as well as the "dielectric" rolls (DR)) are primarily observed in planar layers of calamitic nematics with negative dielectric and positive conductivity anisotropies ($\varepsilon_a<0, \sigma_a>0$). Their main characteristics [the threshold voltage $U_c(f)$ and the critical wave vector $\mathbf{q_c}(f)$] including some frequency-induced morphological transitions (OR→NR→DR at increasing f) are well described by the SM. In contrast to that, an example of nonstandard EC, the LR, is observed in calamitic nematics with $\varepsilon_a<0$, $\sigma_a<0$ [9–12] where no instability should occur at all according to the SM. It has recently been understood that extending the SM by incorporating flexoelectric effects could provide finite threshold voltages for this case and could give an account of the experimental pattern characteristics [13]. Another type of nonstandard EC, the "prewavy" pattern (PW) [14–20], also called wide domains, occurs in calamitic nematics exhibiting standard EC as well. At high frequencies, PW may have a much lower threshold than that provided by the SM (for NR or DR), therefore a morphological transition of DR→PW (or NR→PW) is commonly observed [18,21] at increasing f. In contrast to standard EC, PW is visible only with crossed polarizers. A higher conductivity has been found to promote the formation of the PW pattern by reducing its threshold; however, the formation mechanism of this pattern has not been uncovered yet.

The patterns predicted theoretically [6,8,22,23] and/or found experimentally during the long history of EC in calamitic nematics have one common feature: apart from a low f anomaly in the dielectric regime observed recently in very thin cells [24], their threshold voltages grow with the frequency (i.e., $dU_c/df>0$). As a consequence, experimental studies have rarely been extended to frequencies above 20 kHz [25–27] where EC thresholds typically exceed the upper voltage limit of the available amplifiers and/or the dielectric breakdown voltage of the cells.

Though electroconvection may also occur in bent-core nematics, only a few experiments have been reported so far [5,25,26,28,29]. The compound 4-chloro-1,3-phenylene-bis-4-[4′-(9-decenyloxy)benzoyloxy] benzoate (ClPbis10BB) [5,30], which has been tested in most detail, has exhibited both types of the nonstandard EC introduced above. At low f, nonstandard longitudinal rolls have been seen; at increasing f, however, two prewavy morphologies (PW1 and PW2) have existed which have been

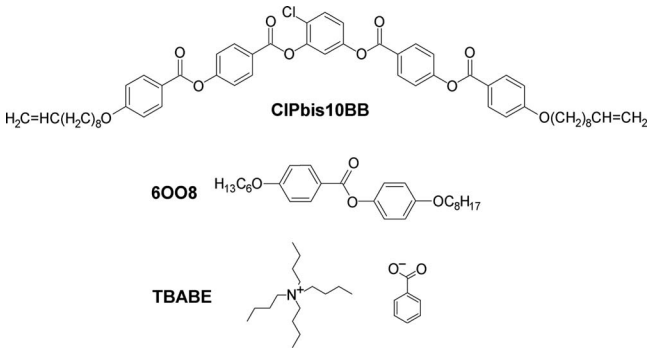

FIG. 1. Chemical structures of the bent-core ClPbis10BB, the rodlike 6OO8 molecules, and the ionic salt TBABE used in the mixtures.

separated by a frequency band where no patterns could be detected at all [refer to Fig. 2(b)]. Their threshold voltages seemed to diverge hyperbolically when approaching this frequency band from any side; otherwise PW1 and PW2 had similar appearance (wavelength, direction, contrast). Unprecedentedly, the higher-frequency PW1 pattern has been characterized by $dU_c/df<0$. A similar behavior has also been reported for another bent-core nematic compound [28]. The reason for these unusual features still awaits exploration.

Mixing compounds of different chemical architecture has proved to be an effective tool to adjust the temperature range and some material parameters of calamitic liquid crystals. One expects that mixing might have similar advantages for bent-core materials too; however, much less efforts have been devoted to such studies so far. Some early trials have indicated only limited miscibilities of banana phases. Recently, binary mixtures of bent-core and calamitic nematics could successfully be prepared where the nematic phase could be preserved in the whole concentration range [31].

In the present paper, we report about electroconvection measurements on these binary mixtures of bent-core and calamitic nematics. In Sec. II, we introduce the substances, the setup, and the measuring method. In Sec. III, we aim to explore how the dilution of the bent-core nematic by a calamitic compound affects the electroconvection thresholds and morphologies. As the magnitude of the electrical conductivity may have a large influence on the EC behavior, in Sec. IV, we construe the consequences of adjusting the conductivity of a selected mixture by doping it with an ionic salt. Finally, we conclude the paper with the discussion in Sec. V.

II. EXPERIMENTAL

The experiments have been carried out on binary mixtures of a bent-core and a calamitic nematic liquid crystal. The well-characterized compound ClPbis10BB [30] has been selected as the bent-core component. As the calamitic constituent of the mixtures, 4-n-octyloxy-phenyl-4'-n-hexyloxybenzoate (6OO8) [32] has been chosen since its structure is similar to that of the arms of the bent-core compound. The chemical structures of these molecules are shown in Fig. 1. The selected compounds are known to exhibit full miscibility, possessing nematic phase at any concentration [31]. Mixtures with three different compositions have been prepared by thorough mixing of the components and letting to homogenize for 1 h in the isotropic phase. The mixtures 7B3R, 5B5R, and 3B7R contained 70, 50, and 30 wt % of the bent-core molecules, respectively. The phase sequences of these mixtures as well as that of the pure compounds are given in Table I.

In order to modify the electrical conductivity of the mixture 7B3R, a doping by the ionic salt tetrabutyl ammonium benzoate (TBABE) in concentrations of 0.01, 0.1, and 1 wt %, respectively, has also been performed. The chemical structure of this dopant is also shown in Fig. 1. The salt was added to the mixture 7B3R in a chloroform solution; after mixing, it was kept at 60 °C for about 2 h in order to let the solvent to evaporate. The measured electrical conductivities of the mixtures (when available) are given in Table I.

In the nematic phase, the dielectric anisotropies ε_a of both the bent-core ClPbis10BB and the rodlike 6OO8 are negative ($\varepsilon_a<0$); the same holds for their mixtures too. The conductivity anisotropy σ_a has, however, a more delicate behavior. As characterized by Wiant *et al.* [5], σ_a of ClPbis10BB changes from negative to positive and then again to negative as the frequency is increased. In the case of 6OO8, according to our preliminary results obtained by a HP4194A Imped-

TABLE I. Composition, electrical conductivity ($\sigma_\perp$ at 80 °C, 1 kHz), and phase sequence of the pure compounds and their mixtures. Cry, Sm–*C*, Sm–C_A, *N*, and *I* denote crystalline, smectic-*C*, anticlinic smectic-*C*, [31], nematic, and isotropic phases, respectively; Sm–*X* is an unidentified smectic phase.

Name	ClPbis10BB (wt %)	6OO8 (wt %)	TBABE (wt %)	$\sigma_\perp$ (Ω^{-1} m^{-1})	Phase sequence and transition temperatures on cooling (°C)
ClPbis10BB	100	0	0	1.6×10^{-7} [5]	Cry 60 *N* 78 *I* [5]
7B3R	70	30	0	2.4×10^{-8}	Sm–*X* 48 Sm–C_A 74 *N* 91 *I*
			0.01		
			0.1	7.5×10^{-7}	
			1	7.5×10^{-6}	
5B5R	50	50	0		Cry 47 Sm–C_A 74 *N* 91 *I*
3B7R	30	70	0	9.9×10^{-9}	Cry 47 Sm–C_A 72 *N* 93 *I*
6OO8	0	100	0	7.9×10^{-9}	Cry 41 Sm–*C* 50 *N* 89 *I*

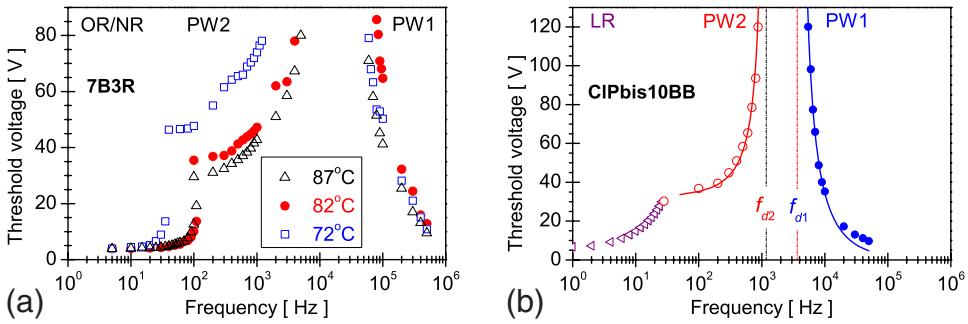

FIG. 2. (Color online) The threshold voltage $U_c(f)$ measured with crossed polarizers in (a) the mixture 7B3R at 87 °C ($T_{NI}-1$ °C), 82 °C ($T_{NI}-6$ °C), and 72 °C ($T_{NI}-16$ °C) in a 20-μm-thick planar cell; (b) in the pure ClPbis10BB at 75 °C ($T_{NI}-3$ °C) (from [5]). PW1 and PW2 denote the high f and the low f prewavy regimes, respectively.

ance gain-phase analyzer comparing the impedances of planar and homeotropic cells, the conductivity anisotropy is negligible at low frequencies (i.e., the parallel and the perpendicular components are almost the same), but becomes clearly positive at high frequencies.

The electroconvection measurements have been performed using either 20-μm-thick commercial [33] or 13-μm-thick homemade cells. Both cell types were constructed from glass substrates covered with etched indium tin oxide (ITO) electrodes and then with antiparallel rubbed polyimide layers to ensure planar orientation. The cells have been filled with the studied mixtures in the isotropic phase and then cooled down slowly to the nematic phase in order to obtain a well-aligned sample. Temperature has been controlled to a precision of 0.1 °C using a hot stage (Instec HS250). EC patterns have been induced by a sinusoidal ac voltage of variable frequency and amplitude which has been applied to the cells from a function generator (Agilent 33120A) through a high-bandwidth high-voltage amplifier. The patterns have been observed by polarizing optical microscopes (Leica DMR XP and Nikon OPTIPHOT-POL) under two crossed polarizers equipped with a digital charge coupled device (CCD) camera for recording snapshot images. The setup allowed to determine the threshold voltages with an experimental error below 5% (including scattering for different cells).

III. DILUTION OF THE BENT-CORE NEMATIC BY CALAMITIC MOLECULES

The EC scenarios have first been tested in 20-μm-thick planar cells of the mixture 7B3R rich in the bent-core component in a very broad (10 Hz–1 MHz) frequency range. The frequency dependence of the threshold voltage $U_c(f)$ of the patterns has been measured at three different temperatures: just below the clearing point ($T=87$ °C$=T_{NI}-1$ °C), in the middle of the nematic range at 82 °C ($T_{NI}-6$ °C), and also close to the nematic-smectic phase transition ($T=72$ °C $=T_{NI}-16$ °C). Here, T_{NI} denotes the nematic-isotropic phase-transition temperature. Patterns belonging to three different morphologies could be detected at each temperature. The frequency ranges for the occurrence of certain pattern types can easily be identified in the $U_c(f)$ plots shown in Fig. 2(a), since the frequency dependence of U_c varies substantially at the morphological transitions. For comparison, $U_c(f)$ of the pure ClPbis10BB is also reproduced from [5] in Fig. 2(b).

At the lowest frequencies ($f \lesssim 100$ Hz), the typical roll patterns (OR or NR) of the conductive regime of standard EC have developed at U_c. Increasing the applied voltage slightly above threshold, the roll patterns become modulated [Fig. 3(a)], forming zigzag structures followed by defect chaos and dynamic scattering at high voltages.

Increasing f, there is a crossover frequency f_c ($f_c \approx 110$ Hz at $T=T_{NI}-6$ °C) where the morphology changes from conductive rolls to a prewavy pattern. In the close vicinity of f_c, the two pattern types coexist in a form of a superposition (defect-free chevron [34]). Above f_c, two different regimes can be distinguished: one (PW2) at lower f up to a few kHz and another (PW1) at high f above 60 kHz. The appearance of the patterns in the two prewavy regimes is almost identical [cf. Figs. 3(b) and 3(c)]: they manifest themselves as wide stripes running normal to the rubbing direction, however, the frequency dependence of their threshold

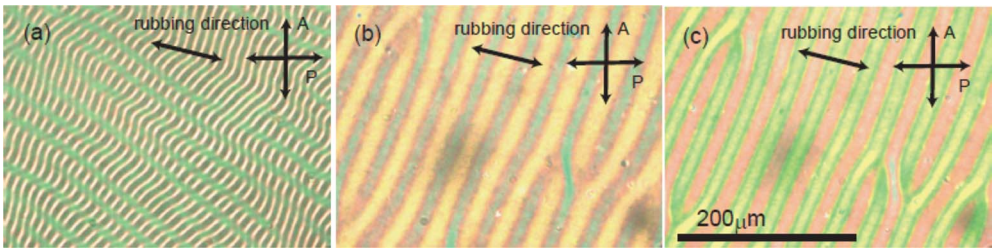

FIG. 3. (Color online) Snapshots of typical electroconvection patterns under crossed polarizers in the nematic phase of the mixture 7B3R (1 °C below the N-I transition). The rubbing direction of the 20-μm-thick planar cell made an angle of 20° with the polarizer. (a) Oblique rolls in the conductive regime at 4 V, 10 Hz; (b) prewavy pattern in the PW2 regime at 50 V, 200 Hz ($U_c=31.1$ V); (c) prewavy pattern in the PW1 regime at 40 V, 200 kHz ($U_c=25.4$ V).

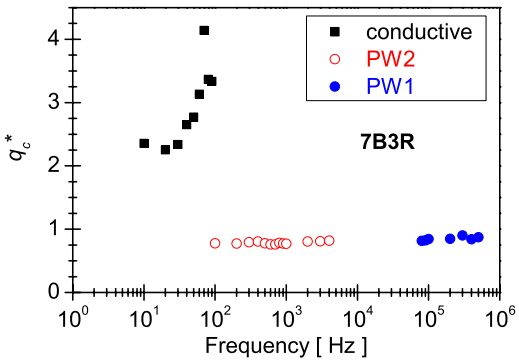

FIG. 4. (Color online) Frequency dependence of the dimensionless wave number q_c^* of the EC patterns in a 20-μm-thick planar cell of the mixture 7B3R.

has an opposite slope [see Fig. 2(a)]. In PW2, the threshold diverges with increasing frequency as $U_c(f) \propto (f_{d2}-f)^{-1}$, while in PW1, the divergence occurs at reducing the frequency as $U_c(f) \propto (f-f_{d1})^{-1}$ (f_{d2}=8.27 kHz, f_{d1}=20.4 kHz at $T=T_{NI}-6$ °C). At voltages much above the threshold, the prewavy pattern transforms into a "wavy" one characterized by sinusoidally modulated disclination loops [14]. In the frequency band $f_{d2}<f<f_{d1}$ separating the two prewavy regimes, no pattern has developed at all.

Comparing the behavior of $U_c(f)$ measured at different temperatures (Fig. 2), one can notice that f_c, marking the crossover between NR and PW2, increases with raising the temperature. In the PW2 regime, higher temperatures resulted in lower threshold voltages as well as in a shift of the lower divergence frequency f_{d2} to larger values. In contrast to that, in the PW1, neither the shift of U_c nor of the upper divergence frequency f_{d1} has exhibited a monotonic behavior with the temperature variation.

For further characterization of the observed patterns, their wavelengths λ have also been determined from snapshots taken at the onset. The dimensionless wave number $q_c^* = q_c d/\pi = 2d/\lambda$ [7] calculated from λ is presented in Fig. 4 for T=82 °C=T_{NI}−6 °C. At low frequencies, $q_c^*(f)$ exhibited a monotonic increase with f; growing sharply in the vicinity of f_c as expected for a conductive EC regime. In contrast to that, in the prewavy regimes, $q_c^*(f)$ had a nearly constant value of about 0.8. It should be emphasized that no significant difference could be found between the q_c^* values of PW1 and PW2 apart from a very weak increase of q_c^* with f valid for both prewavy regimes.

The EC scenarios presented above strongly resemble those reported for the pure ClPbis10BB [5] and shown in Fig. 2(b) to allow easier comparison. Nevertheless, two important differences have to be noticed. The first is a morphological difference: 7B3R exhibits standard conductive rolls at low frequencies, in contrast to the nonstandard longitudinal roll pattern of the pure bent-core nematic. The second is a difference in the frequency ranges. Though the two prewavy regimes separated by a patternless frequency band do exist in ClPbis10BB as well as in the mixture 7B3R, in the latter, they occur at considerably higher frequencies, i.e., both f_{d2} and f_{d1} are about a decade larger in 7B3R than in ClPbis10BB.

In order to investigate the influence of the further reduction of the concentration of the bent-core nematic on the EC scenarios, measurements have been carried out on 20-μm-thick cells filled with the more diluted mixtures of 5B5R and 3B7R, as well as on a 13-μm-thick cell of the pure 6OO8. The threshold voltages determined at T_{NI} −6 °C for all three compounds are presented in Figs. 5(a)–5(c) together with snapshots of characteristic pattern morphologies in Figs. 5(e) and 5(f). The $U_c(f)$ curve for 5B5R shown in Fig. 5(a) still looks quite similar to that of the 7B3R. The conductive rolls at $f \lesssim 150$ Hz followed by a prewavy pattern (PW2) up to 7 kHz do exist in 5B5R; just f_c and f_{d2} are shifted to even higher frequencies compared to 7B3R. The significant difference occurs at high frequencies. Though EC recovers above 100 kHz in 5B5R too and its $U_c(f)$ curve decreases with f similarly to that of the PW1 regime in 7B3R, the morphology of the pattern is completely different. In 5B5R, no prewavy pattern forms at high f, instead a dynamic EC pattern without any periodic stripe structure could be observed [see Fig. 5(d)]. Moving to the mixture 3B7R (which has an even lower concentration of the bent-core molecules), only the two low-frequency pattern types, the conductive rolls and a prewavy pattern, remain observable. It is seen in Fig. 5(b), the crossover frequency shifted up to $f_c \approx 200$ Hz, but the $U_c(f)$ of the prewavy pattern grew much faster with f than in the previous compounds (the upper voltage limit of our amplifier has been reached at considerable lower frequencies) and was not describable by a hyperbolic divergence. The appearance of the prewavy pattern [Fig. 5(e)] was similar to that in the other mixtures and was characterized by similar $q_c^*(f) \approx 0.8$ values. In contrast to the previous mixtures, no electroconvection could be detected above 1 kHz in 3B7R.

Finally, the pure calamitic 6OO8 has also been tested and found to exhibit only standard EC. As seen in the $U_c(f)$ curve shown in Fig. 5(c), the crossover from the conductive regime to the dielectric one occurs at about 200 Hz. The latter is characterized by a square root like $U_c(f)$ and the pattern at onset corresponds to very fine ($\lambda < 3$ μm) dielectric rolls as shown in Fig. 5(f). At high frequencies (above a few kHz), no EC could be detected. We should mention that, though no prewavy pattern could be observed in this sample, raising the voltage much above $U_c(f)$ in the dielectric regime the common dielectric chevron pattern (see Fig. 6) could be induced as a secondary instability. Although some characteristics of the dielectric chevrons (e.g., the azimuthal director modulation in the plane of the surfaces and the large secondary periodicity) may be similar to those of the prewavy pattern (compare Figs. 6(a) and 6(b) to Figs. 3(b), 3(c), and 5(e)], they must not be mistaken. Dielectric chevrons occur as an ordering of defects in the dielectric roll structure (defect mediated chevrons [34]) where the initial rolls still remain detectable as demonstrated in Figs. 6a′ and 6b′ using digital zooming. In contrast to that, rolls with a smaller wavelength have never been detected in the prewavy pattern.

IV. INFLUENCE OF THE CONDUCTIVITY

The studies presented above have convincingly shown that dilution of the bent-core with a calamitic nematic not

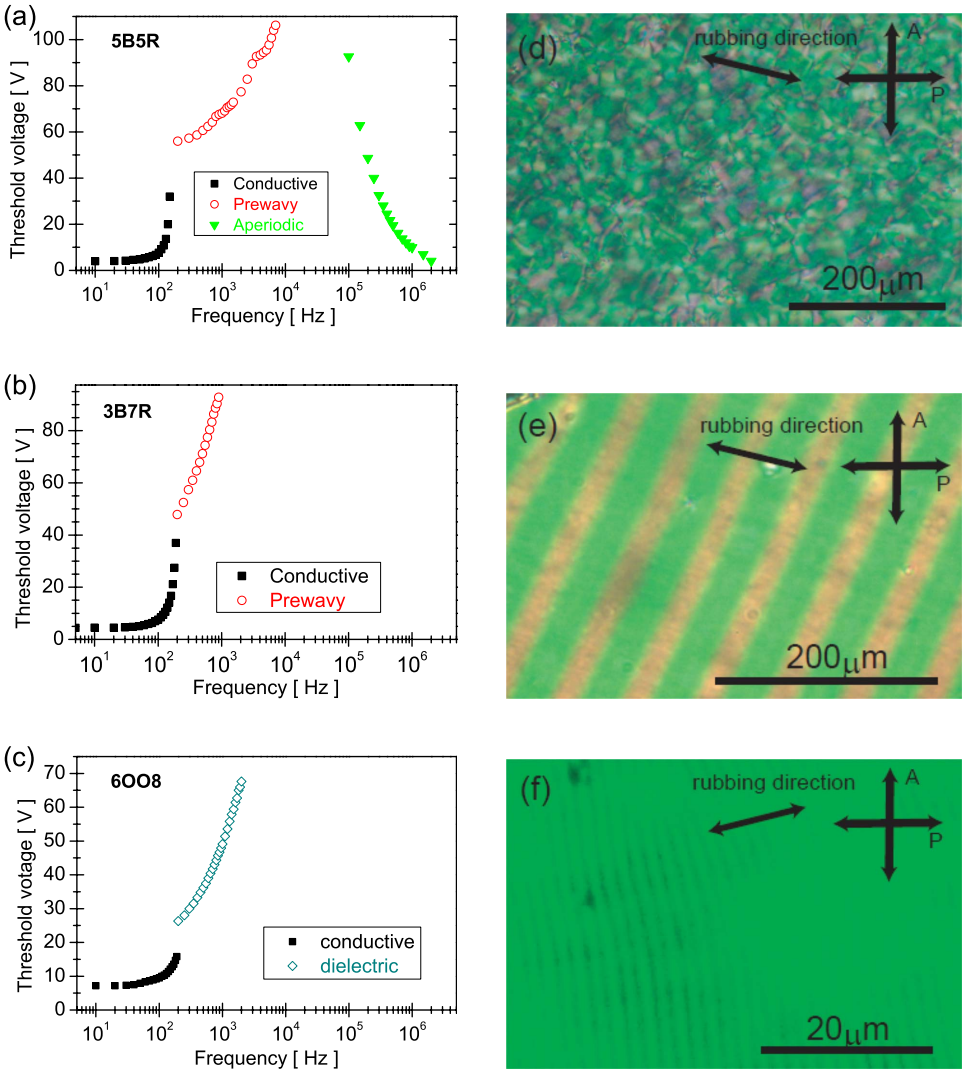

FIG. 5. (Color online) Frequency dependence of the EC threshold voltage $U_c(f)$ and typical EC patterns in the middle of the nematic phase ($T=T_{NI}-6$ °C) (a) in the mixture 5B5R featuring conductive rolls, prewavy pattern, and a dynamic aperiodical convection; (b) in the mixture 3B7R featuring conductive rolls and prewavy pattern but no EC at high frequencies; (c) in the pure calamitic 6OO8 featuring conductive rolls and dielectric rolls but no EC at high frequencies. Snapshot photomicrographs of typical EC patterns at onset taken at crossed polarizers; (d) a dynamic aperiodical convection at 55 V, 500 kHz in 5B5R; (e) the prewavy pattern at 60 V, 250 Hz in 3B7R; (f) dielectric rolls at 42 V, 500 Hz in 6OO8. Please note the changes in the magnification as marked by the scale bars.

only causes quantitative changes in the $U_c(f)$ behavior, but affects the morphology and the existence of EC patterns. At the mixing, the full set of material parameters (elastic moduli, viscosities, conductivity, etc.) changes, therefore it is impossible to conclude which of those parameters is primarily responsible for the changes in the EC scenarios. One of them—the magnitude of the electrical conductivity $\sigma_\perp$—is, however, fairly easily controllable via doping without affecting the other parameters. Threshold voltages of EC patterns are known to be sensitive to the variation of the conductivity; this especially holds for the prewavy regime where a larger $\sigma_\perp$ promotes the occurrence of the pattern by reducing U_c. In addition, it has been found that 6OO8 had a smaller conductivity than ClPbis10BB (see Table I), so reduction of the concentration of the bent-core component was always accompanied by a decrease of $\sigma_\perp$.

Based on these arguments, we have decided to check the direct influence of the conductivity on the EC scenarios by doping the mixture 7B3R with a conductive salt (TBABE, Fig. 1) in various concentrations. Figures 7(b)–7(d) present the frequency dependence of the threshold voltages for 7B3R doped with 0.01, 0.1, and 1 wt % of TBABE, respectively. These measurements have been performed on 20-μm-thick planar cells in the middle of the nematic range at 80 °C. In order to make comparison easier, we have added $U_c(f)$ of the undoped 7B3R obtained at 82 °C in Fig. 7(a). It is common for all four compositions that they exhibit both conductive rolls and prewavy pattern. Increasing the dopant concentration and thus $\sigma_\perp$ the crossover between the two pattern types shifts toward higher frequencies considerably (from 110 Hz to 13 kHz); this corresponds to the expected behavior. In the doped samples, a slight increase of U_c could be detected

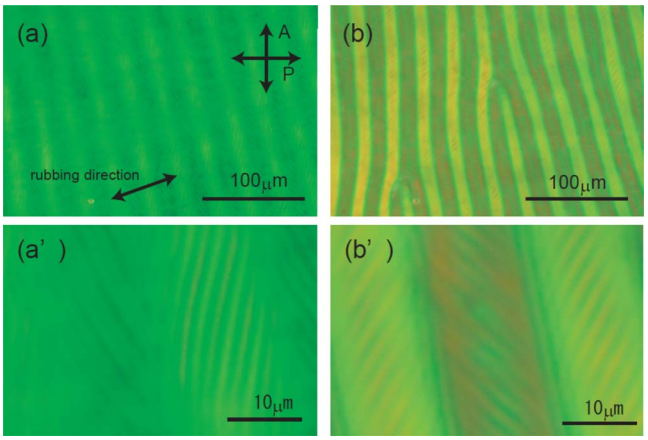

FIG. 6. (Color online) Photomicrographs of the dielectric chevrons in a 13-μm-thick planar cell of the pure rodlike nematic 6OO8 at 80 °C taken under cross polarizers at applied voltages of (a) 46 V, 500 Hz and (b) 49 V, 500 Hz (U_c=36.2 V). (a′) and (b′) are digitally zoomed sections of (a) and (b), respectively, in order to demonstrate the presence of the initial fine dielectric rolls.

when $f \to 0$, which becomes more pronounced at the highest (1 wt %) doping concentration [Fig. 7(d)]. We suggest that this unusual behavior might be related to a big space-charge polarization induced by the large number of ions generated by the added salt [35,36], which may disturb the electroconvective pattern formation.

Doping influences heavily the prewavy regimes too. In the undoped 7B3R, the PW2 and PW1 regimes are clearly separated by a patternless frequency band due to the divergences of $U_c(f)$ [Fig. 7(a)]. In contrast to that, already the lowest (0.01 wt %) dopant concentration makes the prewavy threshold curve continuous [Fig. 7(b)], i.e., the divergences tame down to a maximum. A stronger doping (0.1 wt %) reduces the prewavy thresholds and lowers the maximum value further [Fig. 7(c)]. Finally, at 1 wt % doping the maximum is fully suppressed and $U_c(f)$ becomes flat in the whole prewavy range [Fig. 7(d)].

In the pure ClPbis10BB, it has been found that the temperature dependence of U_c near the clearing point is different in the two prewavy modes (PW2 and PW1) occurring in distinct frequency ranges [5]. This fact has led to the conclusion that the otherwise similar prewavy patterns in these two regimes may be the result of different pattern forming mechanisms whose details still await exploration. On this ground, we have carried out similar studies on the temperature dependence in the undoped and the 0.1 wt % doped 7B3R. In the undoped 7B3R, $U_c(T)$ has been measured at two selected frequencies: at 200 Hz in PW2 and at 200 kHz in PW1 [Fig. 8(a)]. While $U_c(T)$ in PW1 possessed a maximum near the middle of the nematic range, the same in PW2 exhibited a monotonic decrease with an indication of a possible minimum near T_{NI}. This behavior resembles that of the pure ClPbis10BB (see Fig. 9 of [5]) though the change in dU_c/dT for PW1 near the phase transition is much less pronounced in 7B3R. In 7B3R doped with 0.1 wt % TBABE prewavy patterns occur only at higher frequencies and there is no frequency band without pattern. Here, the temperature dependence of the onset voltage at frequencies selected from both sides of the maximum of $U_c(f)$, 50 and 250 kHz, have been compared in Fig. 8(b). Similarly to Fig. 8(a), $U_c(T)$ expresses a maximum for the higher frequency while a monotonic decrease is found for the lower frequency, but the

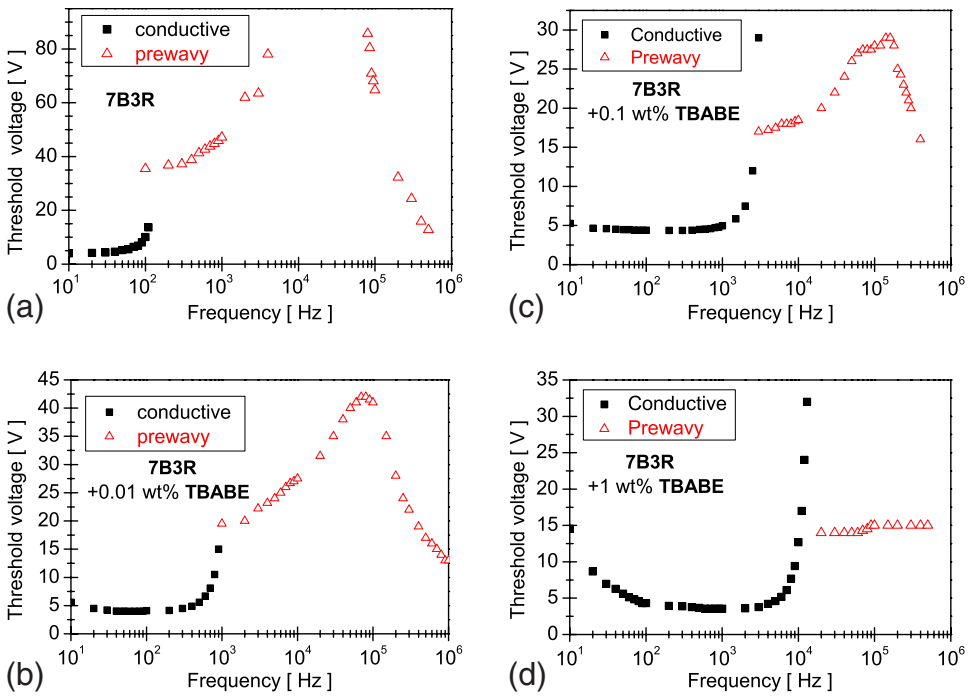

FIG. 7. (Color online) Frequency dependence of the threshold voltage $U_c(f)$ for the (a) undoped 7B3R at 82 °C, (b) 7B3R doped with 0.01 wt % of TBABE at 80 °C, (c) 7B3R doped with 0.1 wt % of TBABE at 80 °C, and (d) 7B3R doped with 1 wt % of TBABE at 80 °C.

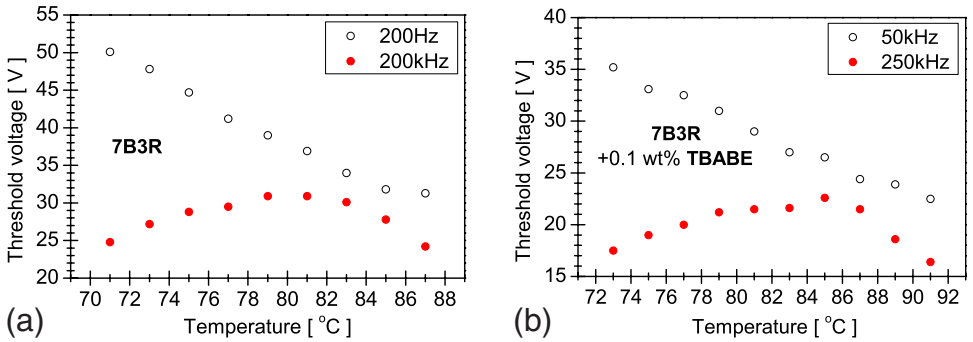

FIG. 8. (Color online) Temperature dependence of the threshold voltage $U_c(T)$ at two frequencies selected from the lower and the higher frequency parts of the prewavy regime, respectively, for (a) the undoped mixture 7B3R and (b) the mixture 7B3R doped with 0.1 wt % TBABE.

change in dU_c/dT close to T_{NI} seems to fade away. Thus, based on the above measurements, we can neither prove nor exclude that in the studied mixtures, the lower frequency ($dU_c/df>0$) and the higher frequency ($dU_c/df<0$) prewavy regimes are the results of different pattern-forming mechanisms.

V. DISCUSSION AND CONCLUSIONS

The existence of EC patterns with relatively low threshold at extremely high frequencies seems to be related to bent-core nematics [5,28] such as ClPbis10BB. Their peculiarity is that they possess a high-frequency prewavy regime (PW1) characterized by the unprecedented $dU_c/df<0$ besides another, low f prewavy regime (PW2) of the common $dU_c/df>0$. The regimes with opposite slope of $U_c(f)$ are assumed to be results of different pattern forming mechanisms whose details are, however, not yet discovered. This behavior abides only in ClPbis10BB/6OO8 mixtures with high concentration of the bent-core component (7B3R), but fades away at increasing the amount of the calamitic nematic; furthermore no PW1-like ($dU_c/df<0$) patterns have been known in calamitic compounds yet. These facts lead to the conclusion that the existence of the dual prewavy regime and especially that of the PW1 mode with $dU_c/df<0$ might be related to the combination of the extraordinary molecular structure and material parameters [37] of the bent-core nematic.

Moreover, we have shown in the doping experiments that the PW1 region tends to disappear with increasing conductivity. In the pure ClPbis10BB and in the undoped 7B3R, the threshold voltages for both PW2 and PW1 diverge, enclosing a frequency band $f_{d2}<f<f_{d1}$ with an infinite pattern threshold [see Figs. 2(a), 2(b), and 7(a)]. Increasing the conductivity may shift the divergence frequencies of the individual modes or weaken their diverging tendency, leading to a turnover $f_{d1}<f_{d2}$. Then the two threshold curves would cross and a change from PW2 to PW1 could occur at finite U_c at a crossover frequency ($\approx 10^5$ Hz) as seen in Fig. 7(b). Increasing the conductivity further [Fig. 7(c)], the crossover frequency shifts to higher values while the threshold decreases, reaching finally a state with a flat $U_c(f)$ in Fig. 7(d). Hence, the initially higher conductivity of the bent-core nematic compared to that of the calamitic compound (Table I) cannot be the cause for the emergence of PW1 with $dU_c/df<0$. On the contrary, the findings could rather be formulated in a way that the effect of the banana-shaped molecules on the EC threshold is suppressed by the increased conductivity.

It should be mentioned that going from Fig. 7(a) to Fig. 7(d), the conductivity has been increased enormously, by 3 orders of magnitude, which shows up also in the shift of the cutoff frequency of the conductive EC regime by about 2 orders of magnitude.

In order to interpret the detected behavior, one can either think of new mechanisms, not included into the standard model (like an isotropic mechanism [23], a special consequence of the unusually large flexoelectric coefficients, electrolytic effects due to the high conductivity [38], etc.) or one could also consider to stay within the frame of the standard model and preserve the inertial term ($\propto f^2$) in the nematohydrodynamic equations [23], which is usually neglected in the theoretical description. Here, it might have a relevance due to the extreme high ($f>100$ kHz) frequencies of the PW1 mode. Detailed elaboration of such models is still a task for the future.

Finally, we would like to mention that not only the pattern morphologies do change when reducing the banana content of the mixture to or below 50%. Recent experiments on the same ClPbis10BB/6OO8 binary system have indicated significant alterations in the dielectric relaxation [39] as well as in x-ray diffraction [40] at about the same concentration range.

ACKNOWLEDGMENTS

The authors are grateful to T. Tóth Katona and J. T. Gleeson for fruitful discussions. Financial support by the Hungarian Research Fund under Grant No. OTKA-K61075 and the Grant-in-Aid for Scientific Research (S) (Grant No. 16105003) from the Ministry of Education, Culture, Science, Sports and Technology of Japan are gratefully acknowledged. S.T., N.É., and K.F.-Cs. are grateful to the hospitality provided by the Research Institute for Solid State Physics and Optics, Budapest and the Tokyo Institute of Technology, respectively, within the framework of a bilateral joint project of the Japanese Society for the Promotion of Sciences and the Hungarian Academy of Sciences.

[1] H. Takezoe and Y. Takanishi, Jpn. J. Appl. Phys., Part 1 **45**, 597 (2006).
[2] L. A. Madsen, T. J. Dingemans, M. Nakata, and E. T. Samulski, Phys. Rev. Lett. **92**, 145505 (2004).
[3] B. R. Acharya, A. Primak, and S. Kumar, Phys. Rev. Lett. **92**, 145506 (2004).
[4] J. Harden, B. Mbanga, N. Éber, K. Fodor-Csorba, S. Sprunt, J. T. Gleeson, and A. Jákli, Phys. Rev. Lett. **97**, 157802 (2006).
[5] D. B. Wiant, J. T. Gleeson, N. Éber, K. Fodor-Csorba, A. Jákli, and T. Tóth-Katona, Phys. Rev. E **72**, 041712 (2005).
[6] L. Kramer and W. Pesch, in *Physical Properties of Liquid Crystals: Nematics*, edited by D. A. Dunmur, A. Fukuda, and G. R. Luckhurst (Inspec, London, 2001), pp. 441–454.
[7] Á. Buka, N. Éber, W. Pesch, and L. Kramer, in *Self-Assembly, Pattern Formation and Growth Phenomena in Nano-Systems*, edited by A. A. Golovin and A. A. Nepomnyashchy, NATO Science Series II, Mathematica, Physics and Chemistry Vol. 218 (Springer, Dordrecht, 2006), pp. 55–82.
[8] L. Kramer and W. Pesch, in *Pattern Formation in Liquid Crystals*, edited by A. Buka and L. Kramer (Springer, New York, 1996), pp. 221–255.
[9] M. Goscianski and L. Léger, J. Phys. (Paris), Colloq. **36**, C1–231 (1975).
[10] L. M. Blinov, M. I. Barnik, V. T. Lazareva, and A. N. Trufanov, J. Phys. (Paris), Colloq. **40**, C3–263 (1979).
[11] E. Kochowska, S. Németh, G. Pelzl, and Á. Buka, Phys. Rev. E **70**, 011711 (2004).
[12] T. Tóth-Katona, A. Cauquil-Vergnes, N. Éber, and Á. Buka, Phys. Rev. E **75**, 066210 (2007).
[13] A. Krekhov, W. Pesch, N. Éber, T. Tóth-Katona, and Á. Buka, Phys. Rev. E **77**, 021705 (2008).
[14] S. Kai and K. Hirakawa, Solid State Commun. **18**, 1573 (1976).
[15] P. Petrescu and M. Giurgea, Phys. Lett. **59A**, 41 (1976).
[16] A. N. Trufanov, M. I. Barnik, and L. M. Blinov, in *Advances in Liquid Crystal Research and Application*, edited by L. Bata, Akadémiai Kidó, Budapest (Pergamon Press, New York, 1980), pp. 549–560.
[17] L. Nasta, A. Lupu, and M. Giurgea, Mol. Cryst. Liq. Cryst. **71**, 65 (1981).
[18] J.-H. Huh, Y. Hidaka, Y. Yusril, N. Éber, T. Tóth-Katona, Á. Buka, and S. Kai, Mol. Cryst. Liq. Cryst. **364**, 111 (2001).
[19] J.-H. Huh, Y. Yusuf, Y. Hidaka, and S. Kai, Phys. Rev. E **66**, 031705 (2002).
[20] J.-H. Huh, Y. Yusuf, Y. Hidaka, and S. Kai, Mol. Cryst. Liq. Cryst. **410**, 39 (2004).
[21] N. Éber and Á. Buka, Phase Transitions **78**, 433 (2005).
[22] L. M. Blinov and V. G. Chigrinov, *Electrooptic Effects in Liquid Crystal Materials* (Springer, New York, 1996).
[23] S. A. Pikin, *Structural Transformations in Liquid Crystals* (Gordon and Breach, New York, 1991).
[24] T. Tóth-Katona, N. Éber, Á. Buka, and A. Krekhov, Phys. Rev. E **78**, 036306 (2008).
[25] P. Kumar, U. S. Hiremath, C. V. Yelamaggad, A. G. Rossberg, and K. S. Krishnamurthy, J. Phys. Chem. B **112**, 9270 (2008).
[26] P. Kumar, U. S. Hiremath, C. V. Yelamaggad, A. G. Rossberg, and K. S. Krishnamurthy, J. Phys. Chem. B **112**, 9753 (2008).
[27] A. N. Trufanov, L. M. Blinov, and M. I. Barnik, Zh. Eksp. Teor. Fiz. **78**, 622 (1980).
[28] S. Tanaka, S. Dhara, B. K. Sadashiva, Y. Shimbo, Y. Takanishi, F. Araoka, K. Ishikawa, and H. Takezoe, Phys. Rev. E **77**, 041708 (2008).
[29] J. Heuer, R. Stannarius, M.-G. Tamba, and W. Weissflog, Phys. Rev. E **77**, 056206 (2008).
[30] K. Fodor-Csorba, A. Vajda, G. Galli, A. Jákli, D. Demus, S. Holly, and E. Gács-Baitz, Macromol. Chem. Phys. **203**, 1556 (2002).
[31] G. G. Nair, C. A. Bailey, S. Taushanoff, K. Fodor-Csorba, A. Vajda, Z. Varga, A. Bóta, and A. Jákli, Adv. Mater. (Weinheim, Ger.) **20**, 3138 (2008).
[32] J. P. van Meter and B. H. Klanderman, Mol. Cryst. Liq. Cryst. **22**, 271 (1973).
[33] Cells supplied by Z. Raszewski, Military Technical Academy, Warsaw.
[34] J.-H. Huh, Y. Hidaka, A. G. Rossberg, and S. Kai, Phys. Rev. E **61**, 2769 (2000).
[35] A. Sawada, Y. Nakazono, K. Tamuri, and S. Naemura, Mol. Cryst. Liq. Cryst. **318**, 225 (1998).
[36] A. Sawada, K. Tamuri, and S. Naemura, Jpn. J. Appl. Phys., Part 1 **38**, 1418 (1999).
[37] A. Jákli, M. Chambers, J. Harden, M. Madhabi, R. Teeling, J. Kim, Q. Li, G. G. Nair, N. Éber, K. Fodor-Csorba, J. T. Gleeson, and S. Sprunt, Proceedings of Emerging Liquid Crystal Technologies III, San Jose, 2008 [Proc. SPIE **6911**, 691105 (2008)].
[38] M. Treiber and L. Kramer, Mol. Cryst. Liq. Cryst. **261**, 311 (1995).
[39] P. Salamon and A. Jákli (private communication).
[40] A. Jákli and S. Sprunt (private communication).